ANALYSIS OF THE MOMENT-OF-FLUID METHOD FOR POLYGONAL MESHES IN AXISYMMETRIC COORDINATE SYSTEM

Konstantin Lipnikov[1] Rao Garimella[1] Angela Herring[3] Eugene Kikinzon[2]
Brendan Krueger[3] Hoby Rakotoarivelo[1] Navamita Ray[2] Mikhail Shashkov[3]
Jan Velechovsky[3]

[1] *Theoretical Division, Los Alamos National Laboratory, Los Alamos, NM, U.S.A.* {*rao,lipnikov,hoby*}*@lanl.gov*
[2] *Computer, Computational and Statistical Sciences Division, Los Alamos National Laboratory, Los Alamos, NM, U.S.A.* {*kikinzon,nray*}*@lanl.gov*
[3] *X-Computational Physics Division, Los Alamos National Laboratory, Los Alamos, NM, U.S.A.* {*angelah,bkkrueger,shashkov,jan*}*@lanl.gov*

ABSTRACT

One of the important features of the arbitrary Lagrangian-Eulerian (ALE) hydrodynamics methods is the appearance of mesh cells containing fractional amounts of more than one material. To resolve sub-scale material dynamics, interfaces between materials inside a cell have to be calculated from material moments. The moment-of-fluid (MOF) method is one of the most accurate interface reconstruction methods. Unlike other methods, it is local and does not require data from neighboring cells which makes it amenable for emerging computer architectures. We analyze this method for axisymmetric problems. Our analysis closes a few gaps in its theoretical justification and provides useful insight on its properties and practical implementation. The theoretical conclusions are confirmed with numerical experiments.

Keywords: interface reconstruction, axisymmetric geometry, polygonal meshes

1. INTRODUCTION

Lagrangian multi-material hydrodynamics methods solve the governing equations on a mesh that moves with the flow and tangles on vorticial and shear flows. To overcome simulation failure due to mesh tangling, a three-step ALE approach is used [1]. First, a Lagrangian calculation that deforms the mesh is performed until the mesh quality falls below an acceptable level. Second, a new mesh with higher quality is created. Third, the physical fields from the deformed mesh are transferred conservatively to the new mesh, a process referred to as remapping. Often it is impractical to preserve material interfaces in the new mesh, since this may require its undesirable refinement. For this reason, many multiphysics codes place multiple materials inside a single computational cell. Such cells are called multi-material cells.

Material distribution inside a multi-material cell is characterized by material moments. Traditionally, hydrodynamics codes use volume-of-fluid (VOF) methods for tracking materials. In these methods only the zeroth-order moments of materials (i.e. simply material volumes) are tracked. Typically, the material volume is normalized by the cell volume and called material volume fraction. Materials such as gases, liquids and solids have different properties, so that accurate simulation of flow requires to resolve dynamics

of materials inside a multi-material cell. This requires to find geometric location of materials and calculate interfaces between them. Recovery of these interfaces from moment data is done by the interface reconstruction (IR) methods. Nowadays, the IR methods are the critical component in predictive ALE modeling of complex multi-material flows.

Knowledge of only material volume fractions gives little information about spatial distribution of materials and leads to a lot of uncertainty in calculating material interfaces. For instance, a linear material interface in a two-material cell cannot be reconstructed uniquely from two volume fractions, see Fig. 6 later. Also, the reconstructed interfaces may depend on the order in which the materials are processed. To reduce uncertainly, most IR methods use information from neighboring cells which increases data movement in a parallel computation and makes the underlying algorithms non-local. The classical VOF method uses gradient of material volume fractions to estimate normal to a material interface in a multi-material cell [2, 3]. After the normal is known, the interface position is defined uniquely by the material volume. Since volume fractions are only weakly connected with the positions of cell centroids (we can change the centroid position without changing the volume fraction), the estimated normal could be quite approximate making the method only first-order accurate.

To reduce uncertainty further, the least squares volume interface reconstruction algorithm (LVIRA) has been developed [4]. This IR method searches for the interface position that cuts off the right volume fraction in the cell of interest and minimizes (in the least square sense) the difference between the given volume fractions in neighboring cells and the volume fractions calculated using this interface. This leads to a nonlinear optimization problem. The LVIRA preserves linear interfaces which is the necessary requirement for a second-order IR method. However, both the VOF and LVIRA methods cannot resolve interface details smaller than a characteristic size of the cell cluster involved in evaluation of the interface normal.

The emerging computer architectures force developers to switch from non-local to local IR methods, preferably flops-intensive. In addition to zeroth-order material moments, these methods use the first-order material moments that are nothing else but material centroids. The focus of this paper is on the moment-of-fluid (MOF) method [5]. Due to data locality, the computational work is performed in a single mesh cell without any interaction with neighbors which makes this IR method amenable for novel computing platforms. The MOF can resolve interface details smaller than the computational cell such as in thin material layers.

Other non-local IR methods are the Youngs [6], ELVIRA [7], and Swartz [8] methods. They have the same fundamental deficiencies as the VOF and LVIRA. Other local IR methods are the symmetric MOF [9] and xMOF [10].

In practice, many important problems can be studied under assumption of the cylindrical symmetry, e.g. a liner implosion in ICF simulations [11]. This assumption leads to a 2D problem posed in the RZ (axisymmetric) coordinate system which saves a lot in computational cost. A few papers consider extension of the MOF to the RZ coordinate system [12] without paying enough attention to its theoretical justification. *This work closes a few gaps in the theory.* In particular, the uniqueness and stability results help development and analysis of robust converging numerical methods. For example, the uniqueness result (see Lemma 1) implies that the underling nonlinear optimization problem has an unique global minimum. Hence, linear interfaces can be recovered uniquely which allows us to resolve accurately thin material layers inside a multi-material cell. None of the non-local IR methods has this potential existing in the MOF method.

Note that some of the theoretical results considered here were formulated, but not proven, earlier for the Cartesian coordinate system, see [5]. Our analysis closes the existing theoretical gaps and shows the differences and commonalities between MOF methods in the 2D Cartesian and RZ coordinate systems that could be used in writing efficient codes.

The MOF method requires three times more data than the VOF method, both in terms of storage and overhead with respect to updating the material centroids. This additional cost should be weighted against the remap frequency in an ALE simulation, the complexity of this simulation, and additional accuracy provided by the MOF method. Also, the cost of the MOF method grows significantly with the number of materials in a cell. To reduce the cost, analytical formulae for cutting a given volume fraction are derived in [13]. Another way to quickly find the position of a cut-off line is the Newton-type method proposed in [14]. Efficient analytic formulae for calculating objective functional on hexahedral meshes are proposed in [15].

All numerical experiments are performed using the Portage code [16]. This is an open-source, scalable and extensible data transfer (remap) library for numerical simulations. It supports state-of-the-art remap schemes for meshes and particles in 2D and 3D up to a second-order accuracy. Portage ensures critical properties such as local/global conservation laws and bounds preservation for remapped fields. It enables multi-material field remap through the use of a dedicated interface reconstruction plugin, Tangram, and leverages the hybrid parallelism exposed by ad-

vanced architectures using multi-processing and multi-threading.

The paper outline is as follows. In Section 2, we describe polygonal meshes in the RZ coordinate system. In Section 3, we formulate and prove a few theoretical results that underpin the successful behavior of the MOF method in practice. In Section 4, we summarize the code implementation of the IR methods. In Section 5, we verify our finding with numerical experiments in the RZ coordinate system.

2. POLYGONAL MESHES IN THE RZ COORDINATE SYSTEM

Polygonal cells appear naturally in various multi-physics multi-material simulations ranging from flow and reactive transport in fractured rock to compressible gas and material flows in hydrodynamics. Polygonal meshes are useful for modeling dynamic opening (or closure) of fractures via splitting (or merging) cells of a background mesh. In hydrodynamics, polygonal cells appear in the ALE framework as a way to compromise between improving mesh quality and preserving some flow features [17].

Other sources of polygonal meshes are the adaptive mesh refinement methods. A locally refined mesh may be considered as the conformal polygonal mesh with degenerate cells (for instance, when the angle between two neighboring faces in a cell is zero). Usage of such degenerate (but shape-regular) polygonal cells allows us to avoid superfluous mesh refinement. Any definition of a cell shape-regularity could be used. To be precise, hereafter, we assume that a shape-regular polygon could be split into the uniformly bounded number of triangles that are shape-regular in the sense of Ciarlet.

In contrast to Voronoi meshes (see e.g., [18] and references therein), arbitrary polygonal meshes provide greater flexibility for meshing complex domains. For instance, badly shaped (needle-type) triangles could be simply merged with their neighbors forming a shape-regular polygon.

Since the RZ coordinate system mimics a 3D geometry, we will use volumes in the subsequent discussion. However, we will use cut-off line since geometric operations are done in two-dimensions. The volume of cell Ω is defined as follows:

$$|\Omega| = \int_\Omega \mathrm{d}V, \quad \mathrm{d}V = r\mathrm{d}r\mathrm{d}z.$$

Its centroid is defined as

$$\mathbf{x}_\Omega = \frac{1}{|\Omega|}\int_\Omega \mathbf{x}\ \mathrm{d}V.$$

The norm of the position vector $\mathbf{x} = (r,\, z)$ is defined as

$$\|\mathbf{x}\| = \sqrt{r^2 + z^2}.$$

Observe that the only difference with similar definitions in the Cartesian coordinate system is in the use of the infinitesimal volume $\mathrm{d}V$. This implies that many algorithms could be written and analyzed in the geometry-agnostic way.

3. MOMENT-OF-FLUID METHOD

3.1 Two-Material Problem

The case of two materials in a single cell provides useful insight on the interface reconstruction problem. For simplicity, we consider a convex cell which is a typical assumption for many Lagrangian hydrodynamic applications. It allows us to control (to some extend) properties of the deformation tensor, such as positivity of the Jacobian. Throughout this section, we try to use geometry-independent arguments; so that the conclusions could be applied to both the 2D Cartesian and RZ coordinate systems.

We will use the following definitions. The symmetric difference for two polygonal domains ω_1 and ω_2 is defined as follows:

$$\Delta(\omega_1, \omega_2) = (\omega_1 \cup \omega_2)/(\omega_1 \cap \omega_2). \tag{1}$$

3.1.1 Theoretical Background

The theoretical background for interface reconstruction method is based on the fact that some parts of a polygonal cell could be uniquely characterized by their centroid.

Let Ω be a convex polygon cut into two polygons ω_1 and ω_2 by a cut-off line ℓ. Let $\mathbf{x}_{\omega_1}$ and $\mathbf{x}_{\omega_2}$ be centroids of the two polygons. The definition of the centroid and $|\Omega| = |\omega_1| + |\omega_2|$ give

$$\mathbf{x}_\Omega = \frac{1}{|\omega_1| + |\omega_2|}\left(\int_{\omega_1} \mathbf{x}\ \mathrm{d}V + \int_{\omega_2} \mathbf{x}\ \mathrm{d}V\right).$$

The integrals can be computed exactly by evaluating $\mathbf{x}$ at the centroids two polygons. This leads to the following formula:

$$\mathbf{x}_\Omega = \mathbf{x}_{\omega_1} f_1 + \mathbf{x}_{\omega_2}(1 - f_1), \quad f_1 = |\omega_1|/|\Omega|. \tag{2}$$

Thus, the centroid of cell Ω lies on the line connecting the centroids of its pieces. This is true for any object split into two pieces. We will use this fact later. Position of the cut-off line ℓ is defined by the vector $\mathbf{n}$ normal to it, see Fig. 1. Equivalent definition is the distance d to the cut-off line which is $d = \|\mathbf{n}\|$ and the angle φ between $\mathbf{n}$ and the r-axis.

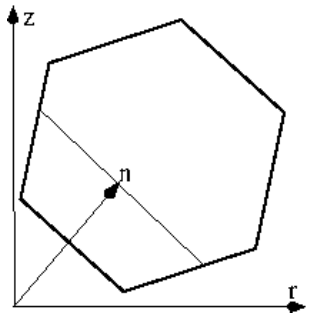

Figure 1: The RZ coordinate system: Position of the cut-off line ℓ is defined by the normal vector $\mathbf{n}$.

Let μ^* be the volume of ω_1. In analysis, we often assume that μ^* is *fixed* and

$$0 < \mu^* < |\Omega|.$$

Strict inequalities allow us to avoid empty polygons and one-material cells. We use $\ell(\mu^*)$ to denote any line cutting a polygon with volume μ^*.

In a few papers on IR methods, the following uniqueness result is formulated without a proof for the Cartesian coordinate system. For instance, the following statement is made in [5]: "Property 1. Each truncation volume is uniquely identified by its centroid." In our opinion this statement is somewhat intuitive but not obvious at all.

Lemma 1. Let Ω be a convex cell and $\mathbf{x}_{\omega_1}$ be the centroid of a non-empty polygon ω_1 cut off by a line ℓ. Then, the position of centroid $\mathbf{x}_{\omega_1}$ identifies the unique cut-off line ℓ.

Proof. Let us assume the opposite that there exist two different cut-off lines ℓ and $\tilde{\ell}$ and two different cut-off polygons ω_1 and $\widetilde{\omega}_1$ with the same centroid $\mathbf{x}_{\omega_1}$. The left panel in Fig. 2 shows the case when the cut-off lines do not intersect inside Ω. Since either $\widetilde{\omega}_1$ includes strictly ω_1 or vise versa, the centroids must be different due to property (2).

The case of intersecting cut-off lines is more involved. Let ω_c be the common part of the two polygons, $\omega_c = \omega_1 \cap \widetilde{\omega}_1$, with centroid $\mathbf{x}_c$. Since $\omega_1 = \omega_c \cup \omega_a$ and $\widetilde{\omega}_1 = \omega_c \cup \widetilde{\omega}_b$, we have

$$\mathbf{x}_{\omega_1} = \mathbf{x}_c f_c + \mathbf{x}_a(1 - f_c) = \mathbf{x}_c \tilde{f}_c + \mathbf{x}_b(1 - \tilde{f}_c), \quad (3)$$

where f denotes the volume fraction, like in (2), e.g. $f_c = |\omega_c|/|\omega_1|$. Hence $(\mathbf{x}_a - \mathbf{x}_c)(1 - f_c) = (\mathbf{x}_b - \mathbf{x}_c)(1 - \tilde{f}_c)$. Let $\mathbf{p}$ be the intersection point of two cut-off lines ℓ and $\tilde{\ell}$. Due to convexity of all polygons the line defined by points $\mathbf{p}$ and $\mathbf{x}_c$ separates strictly ω_a and ω_b. Hence the vectors $\mathbf{x}_a - \mathbf{x}_c$ and $\mathbf{x}_b - \mathbf{x}_c$ cannot be collinear. This contradiction proves the assertion of the lemma. □

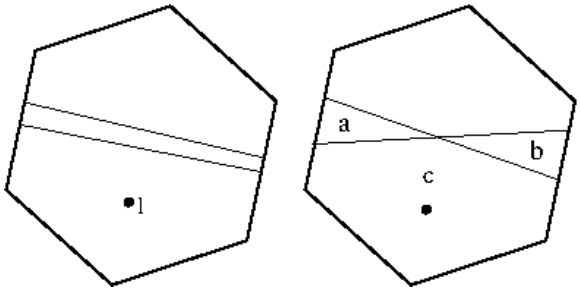

Figure 2: Partitioning of cell Ω by two cut-off lines ℓ and $\tilde{\ell}$. The solid bullet is the common centroid of polygons ω_1 and $\widetilde{\omega}_1$.

The above lemma allows us to define a map $\mathcal{M}\colon \mathbf{x}_{\omega_1} \to \omega_1$, where $\mathbf{x}_{\omega_1} \in \Omega$ is an interior point. Since for a given non-empty ω_1, we have the formula for its centroid, the map is bijective. Let us consider subset of polygons ω_1 with fixed volume μ^* and denote the corresponding restriction of the map by $\mathcal{M}(\mu^*)$. In optimization algorithms, mentioned below, we need to control the inverse of this map.

Lemma 2. The map $(\mathcal{M}(\mu^*))^{-1}$ is continuous.

Proof. Let ω_1 and $\widetilde{\omega}_1$ have the same volume μ^*. Then, the difference between their centroids is

$$\|\delta\mathbf{x}\| = \|\frac{1}{\mu^*}\Big(\int_{\widetilde{\omega}} \mathbf{x}\,\mathrm{d}V - \int_{\omega} \mathbf{x}\,\mathrm{d}V\Big)\| \le \frac{R}{\mu^*}|\delta\omega|,$$

where R is the maximum norm of $\mathbf{x}$ in Ω, and $\delta\omega$ is the symmetric difference of ω_1 and $\widetilde{\omega}_1$, see (1). Since μ^* is fixed, the assertion of the lemma follows immediately. □

This lemma implies that any numerical implementation of optimization algorithms that vary orientation of the normal vector $\mathbf{n}$ should take into account sensitivity to small volumes μ^*. The problem is slightly mitigated by observing that $|\delta\omega| \sim S\|\delta\mathbf{n}\|$ where is S is the area of the cut-off line inside Ω.

Understanding the accuracy of the interface reconstruction is important for the development of new IR methods. The above uniqueness result implies that a linear interface is recovered exactly. This is the necessary condition for a second-order method.

Preservation of material volume is paramount in practical applications. However, Lemma 1 cannot be generalized to include volume fraction constraints. We need to complement it with the following approximation result.

Lemma 3. Let Ω be a convex cell containing two simply-connected physical material regions $\widetilde{\omega}_i$ with the C^2-continuous interface between them. Furthermore, let $\widetilde{\omega}_1$ be star-shaped with respect to its centroid $\mathbf{x}_{\widetilde{\omega}_1}$.

Finally, let ω_1 be a polygonal approximation of $\widetilde{\omega}_1$ with the same centroid and having the same volume fraction. Then, ω_1 is the second-order approximation of $\widetilde{\omega}_1$.

Proof. Let us consider the case when the cut-off line ℓ intersects the material interface in only one point, $\mathbf{p}$, see the left panel in Fig. 3. We re-use the arguments from Lemma 1. Formula (3) holds true and implies that vectors $\mathbf{x}_a - \mathbf{x}_c$ and $\mathbf{x}_b - \mathbf{x}_c$ must be collinear. Moreover, if $f_c > \tilde{f}_c$, then

$$\mathbf{x}_c(f_c - \tilde{f}_c) + \mathbf{x}_a(1 - f_c) = \mathbf{x}_b(1 - \tilde{f}_c).$$

Hence, $\mathbf{x}_b$ is the convex combination of $\mathbf{x}_c$ and $\mathbf{x}_a$. This is not possible since ω_1 is convex and contains the whole segment from $\mathbf{x}_c$ to $\mathbf{x}_a$. All points of this segment are separated from $\mathbf{x}_b$ by the cut-off line.

If $f_c < \tilde{f}_c$, $\mathbf{x}_a$ is the convex combination of $\mathbf{x}_c$ and $\mathbf{x}_b$. Since $\mathbf{x}_{\widetilde{\omega}_1}$ is also the convex combination of $\mathbf{x}_c$ and $\mathbf{x}_b$, we have four points lying on one line and we know their order. Indeed,

$$\mathbf{x}_{\widetilde{\omega}_1} = \mathbf{x}_c\tilde{f}_c + \mathbf{x}_b(1 - \tilde{f}_c),$$
$$\mathbf{x}_a = \mathbf{x}_c\frac{\tilde{f}_c - f_c}{1 - f_c} + \mathbf{x}_b\frac{1 - \tilde{f}_c}{1 - f_c}.$$

Note that $\tilde{f}_c$ is bigger than the coefficient in front of $\mathbf{x}_c$ in the second equation. Thus $\mathbf{x}_{\omega_1}$ is closer to $\mathbf{x}_c$ than $\mathbf{x}_a$. Since the material polygon is star-shaped with respect to its centroid, points $\mathbf{x}_a$ and $\mathbf{x}_b$ are not separated by the line connecting $\mathbf{x}_{\widetilde{\omega}_1}$ with $\mathbf{p}$, but regions ω_a and ω_b are separated by this line. We have a contradiction, so the one-point intersection case is not possible.

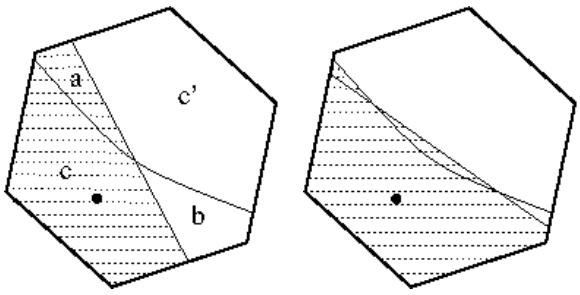

Figure 3: Cell Ω with the curved material interface. The solid bullet is the common centroid of polygon ω_1 that is shaded and material region $\widetilde{\omega}_1$.

Let now consider the case of two (or more intersections), see the right panel in Fig. 3. Since the material interface is C^2, any cut-off line intersecting it in at least two places approximates it with the second order accuracy. This proves the assertion of the lemma. □

Unfortunately, we cannot drop the C^2 interface regularity assumption. For instance, when the interface has a sharp kink, its linear approximation will be only first-order accurate.

3.1.2 Constrained Problem

When the material interface in a cell is a straight line, the uniqueness result of Lemma 1 implies that the material volume is preserved exactly. This is no longer true for a general curved interface, where the volume of a cut-off polygon ω_1 is not guaranteed to match the volume of the corresponding physical material $\widetilde{\omega}_1$. Also, in practice, the material centroid is defined approximately, upto a discretization error which introduces noise in the input data. In contrast to material centroid, material volume is directly connected to the mass conservation law and must be preserved in a discrete algorithm.

Let $\widetilde{\omega}_i$ denote two material regions in cell Ω with approximate centroids $\mathbf{x}_{\widetilde{\omega}_i}$. We call these centroids the target centroids. The constrained interface reconstruction problem is to find a cut-off line that cuts the prescribed material volumes $|\widetilde{\omega}_1| = \mu^*$ and minimizes deviation of centroids $\mathbf{x}_{\omega_i}$ from the target centroids. For a two-material problem it is sufficient to consider only one centroid:

$$\omega^* = \min_{\omega \in \mathcal{F}(\mu^*)} \|\mathbf{x}_{\omega_1} - \mathbf{x}_{\widetilde{\omega}_1}\|^2, \tag{4}$$

where $\mathcal{F}(\mu^*)$ is the set of admissible polygons:

$$\mathcal{F}(\mu^*) = \{\omega\colon\ \omega \subset \Omega,\ |\omega| = \mu^*\}.$$

This is a non-linear optimization problem with 2 unknowns, components of vector $\mathbf{n}$, representing the position of the cut-off line.

The proof of the following result has been sketched in [5] for the Cartesian coordinate system. Our proof is more complete and works for both the Cartesian and axisymmetric coordinate systems.

Lemma 4. The constrained interface reconstruction problem (4) has a solution.

Proof. Note that ω is defined uniquely by its cut-off line ℓ; hence, by its position vector $\mathbf{n}$. We say that $\omega = T(\mathbf{n})$. Then, optimization problem (4) can be reformulated as the optimization problem over subset $T^{-1}(\mathcal{F}(\mu^*)) \subset \Re^2$. This subset is obviously bounded. It is also closed since $\mathbf{n}_i \to \mathbf{n}$ implies $|T(\mathbf{n})| = \mu^*$. Hence $T^{-1}(\mathcal{F}(\mu^*))$ is compact. Then, the minimum exists by the Weierstrass theorem. □

The following optimization algorithm searches for a local minimum of the objective functional. First, we represent $\mathbf{n}$ as the pair (d, φ), where $d = \|\mathbf{n}\|$ and φ is the angle between $\mathbf{n}$ and the r-axis.

1. Find initial guess φ^0 using direction $\mathbf{x}_\Omega - \mathbf{x}_{\omega_1}$.

2. Find an interval (φ_l, φ_u) that contains φ^0 and has a local minimum of the objective functional.

3. Find the local minimum using a gradient descent method.

The last two steps require multiple evaluations of the objective functional. Each such evaluation requires us to find a cut-off line normal to $\mathbf{n}^k$ that cuts polygon ω_1^k with volume μ^*. For a fixed φ^k, the volume of this polygon is a monotone function of d. Thus, the required value of d^k can be found using either analytic (e.g. [13]) or iterative (e.g. [14]) methods.

3.2 Generalization to Multiple Materials

Consider the case of M materials, $M > 2$. For the case of multiple materials, we solve the following local optimization problem with $2(M-1)$ unknowns representing normals to $M-1$ cut-off lines ℓ_i:

$$\{\omega_i^*\}_{i=1}^M = \min_{\{\omega_i\}\in\mathcal{G}} \sum_{i=1}^{M} \|\mathbf{x}_{\omega_i} - \mathbf{x}_{\widetilde{\omega}_i}\|^2,$$

where $\mathcal{G}$ is the set of partitions of Ω into M polygons with prescribed volumes $\{\mu_i^*\}_{i=1}^M$. As before, we can exclude one term from the objective functional.

Note that the MOF method is intrinsically the two-material IR method. Thus, the problem with many materials should be reduced to a set of two-material sub-problems by grouping the materials. To find the global minimum, we need to consider all possible groups. For each group, we use formula (2) to calculate the group centroid.

The grouping algorithm is obviously recursive and the total number of two-material problems is $M!/2$. Thus, the cost of MOF grows quickly for large M which opens room for future analysis of global optimization methods such as the simulated annealing and the active particles matter.

The MOF method is exact when the interfaces between all two-material groups are linear. Finally note that the MOF does not need to know the order of materials to find their configuration inside a cell; although, this comes with the increased combinatorial cost.

4. PACKAGE IMPLEMENTATION

The IR methods are implemented in the Tangram module (available from github.com/larista/tangram) of the data transfer package Portage (available from github.com/larista/portage). Software design of this package can be found in [16].

4.1 Portage

Portage is the actively developed open source library that implements locally conservative data transfer (remap) algorithms. It provides a lightweight and extensible interface that can easily be customized and integrated into simulation codes. Portage supports general polytopal meshes and provides second-order accurate bounds-preserving remap algorithms. It provides intersection-based, swept-face based and particle-based remap algorithms.

Portage is designed to scale to thousands of cores on distributed architectures through MPI and OpenMP, with support for GPUs in development. Unlike other similar monolithic libraries, Portage is a framework for creating custom remappers from interoperable components that can be mixed and matched as long as they adhere to Portage's API. Finally, its design seeks to minimize the amount of mesh and field data that must be copied from client application.

4.2 Tangram

Tangram is the IR module inside Portage and provides most of the IR methods discussed in the Introduction. Tangram is also composed of interoperable modules such as Clipper and Splitter. The Clipper computes the aggregated moments of materials below the cut-off line. Splitter splits a polygon by a cut-off line. The result is two sets of convex polygons, one corresponds to materials above the cut-off line, and the other to the materials below it. Each set contains the zero-order and first-order moments.

Tangram provides custom implementation of the Clipper and Splitter components using the R2D package [19] and the nested dissection algorithm. The R2D package provides the basis capability of clipping a non-convex polygon with a line.

5. NUMERICAL EXAMPLES

Our primary objective is to verify the conclusions we made in the theoretical section; hence, we do not perform extensive numerical experiments for various material configurations. For such experiments, we refer the reader to the previous papers on the subject. Hereafter, the input moments are computed via exact (or very accurate) integration over intersection regions between materials and mesh cells. The secondary objective is to demonstrate correctness of the Portage-Tangram implementation of the RZ coordinate system.

5.1 Linearity preservation

Consider the case of three materials (red, cyan, yellow) with linear interfaces. In this case there exists one grouping of materials where the groups are separated by straight lines. According to Lemma 1, the MOF method should preserve linear interfaces exactly provided that the input data (material volume fractions and material centroids) are also exact.

First we consider a square mesh shown in Fig. 4. There is only one mesh cell with three materials in it. The VOF method is not expected to be exact in such a case; however, this cell impacts accuracy of the interface reconstruction algorithms in the neighboring cells. The MOF algorithm provides exact solution up to the tolerances specified in Tangram. We did not observe algorithm sensitivity to small volumes discussed after Lemma 2, which implies that a sharper result could be proven.

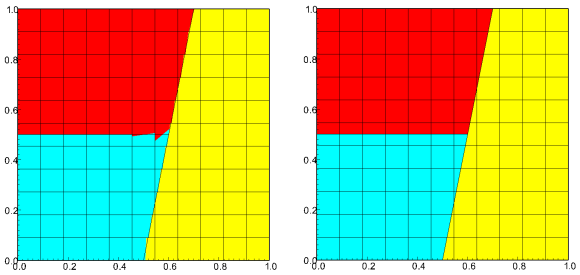

Figure 4: Comparison of the VOF (left panel) and MOF (right panel) methods on the square mesh.

Now we repeat the experiment but on a polygonal mesh built as follows. First, we define a set of points $\mathbf{x}_{i,j} = (r_{i,j}, z_{i,j})$ for generating the Voronoi tessellation:

$$r_{i,j} = \xi_i + 0.1 \sin(2\pi\xi_i) \sin(2\pi\eta_j),$$
$$z_{i,j} = \eta_j + 0.1 \sin(2\pi\xi_i) \sin(2\pi\eta_j),$$

where $\xi_i = ih$, $\eta_j = jh$ and $h = 1/n$. Then, a median mesh is constructed from the Voronoi mesh by moving each mesh vertex to the center of a triangle formed by the centers of three Voronoi cells sharing the vertex.

Notice that the VOF produces one material triangle in three-material cell whose orientation is significantly misaligned with the bulk material (see red material in Fig. 6). The MOF method preserves linearity even in cells attached to the axis of symmetry ($r = 0$). Using the sequence of polygonal meshes, we again did not observe any sensitivity of the IR algorithms to small volumes.

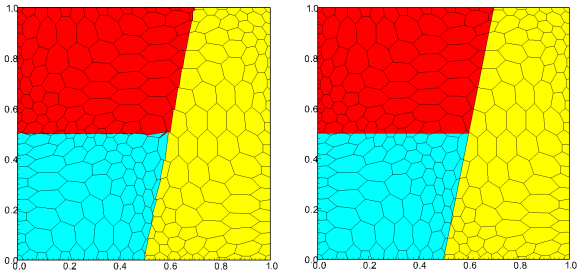

Figure 5: Comparison of the VOF (left panel) and MOF (right panel) methods on the polygonal mesh.

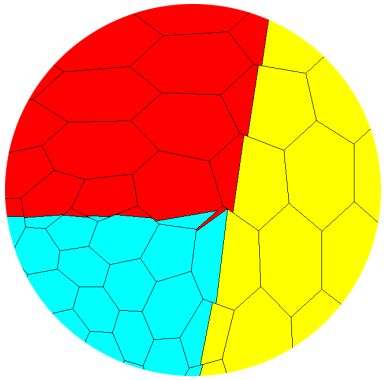

Figure 6: Zoom on the interface details in the VOF method from Fig. 5.

5.2 Second-order accuracy

Now we consider the two-material problem in the RZ coordinate system. The first material is the disk of radius 0.3 centered at the middle of the unit square domain, see Fig. 7.

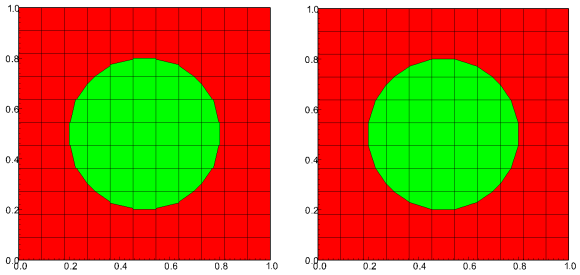

Figure 7: Approximation of the disk using the VOF (left panel) and MOF (right panel) methods.

We use a symmetric difference to quantify the IR error. The total error for material 1 is defined at the sum of measures of symmetric differences in all multi-material cells. The results of numerical experiments on

a sequence of square meshes are collected in Table 1. We use the linear regression algorithm to calculate the convergence rates. As expected, VOF is the first-order method and MOF is the second-order method. We do not observe any superconvergence of the VOF method despite high regularity of the underlying mesh.

mesh	VOF	MOF
11x11	7.26e-3	4.53e-3
22x22	4.12e-3	1.22e-3
44x44	1.98e-3	2.62e-4
88x88	1.18e-3	8.28e-5
rate	0.89	1.95

Table 1: Convergence rates for various IR methods on the sequence of square meshes.

Now we repeat the experiment on the sequence of polygonal meshes with the characteristic mesh size h, see Fig. 8 and Table 2. Note that the VOF method shows some super-convergence that could be attributed to mild regularity of the polygonal mesh. In contrast to the square mesh, smaller number of neighbors participate in calculating interface normals which leads to sharper results. The MOF is second-order accurate as predicted in Lemma 3.

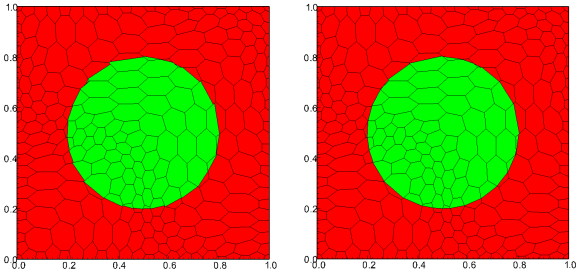

Figure 8: Approximation of the disk with the VOF (left panel) and MOF (right panel) methods.

1/h	VOF	MOF
16	7.87e-3	4.79e-3
32	2.32e-3	1.16e-3
64	8.33e-4	2.58e-4
128	3.78e-4	6.37e-5
rate	1.46	2.09

Table 2: Convergence rates for various IR methods on the sequence of polygonal meshes.

5.3 Approximate centroids

Now we add random noise to material centroids. This mimics a flow simulation scenario where the position of centroids is known upto a discretization error. We assume the second-order discretization error and perturb centroids using random variable between -0.25 to 0.25 multiplied by the material volume. The errors based on measuring the symmetric differences are shown in Table. 3 The errors are larger than before but the method remains second-order accurate.

square meshes		polygonal meshes	
1/h	MOF	1/h	MOF
11	7.47e-3	16	5.75e-3
22	2.06e-3	32	1.44e-3
44	3.50e-4	64	3.41e-4
88	1.13e-4	128	7.73e-5
rate	2.07		2.07

Table 3: Convergence rates for the MOF with random perturbation of centroids.

6. SUMMARY

We revisited the theoretical background of the MOF interface reconstruction method and generalized known results from the Cartesian to the RZ coordinate system. We proved results that were previously stated for the Cartesian coordinate system as unproved propositions. These proofs are novel and provide useful insight on the properties of the MOF method.

We compared local (VOF) and non-local (MOF) IR methods. Although, it is known that VOF's performance is inconsistent and unpredictable, we observed its super-convergence in a few cases. As the rule of thumb, we expect good results from the VOF for the two-material case with a planar interface on a regular grid and away from the boundary and material cross points.

The MOF method remained second-order accurate in all cases including the case of second-order random perturbation of material centroids. The guaranteed linearity preservation property of the MOF method in the case of multiple materials makes this method most suitable for multi-material ALE simulations.

References

[1] Barlow A., Maire P.H., Rider W., Rieben R., Shashkov M. "Arbitrary Lagrangian–Eulerian methods for modeling high-speed compressible multimaterial flows." *J. Comput. Phys.*, vol. 322, 603–665, 2016

[2] Hirt C., Nicholas B. "A computational method for free surface hydrodynamics." *J. Pressure Vessel Technology*, vol. 103, 136, 1981

[3] Rider W., Kothe D. "Reconstructing volume tracking." *J. Comput. Phys.*, vol. 141, 112–152, 1998

[4] Puckett E.G. "A Volume-of-fluid Interface Tracking Algorithm with Applications to Computing Shock Wave Refraction." *Proceedings of the Fourth International Symposium on Computational Fluid Dynamics*, pp. 933–38. 1991

[5] Dyadechko V., Shashkov M. "Moment-of-fluid interface reconstruction." Tech. Rep. LAUR-05-7571, Los Alamos National Laroratory, 2005

[6] Youngs D. "Time-dependent multi-material flow with large fluid deformation." *Numerical Methods for Fluid Dynamics*, pp. 273–285. Academic Press, 1982

[7] Pilliod J. *An analysis of piecewise linear interface reconstruction algorithms for volume-of-fluid methods.* Master's thesis, Univ. of California, Davis, 1992

[8] Swartz B. "The second-order sharpening of blurred smooth borders." *Math. Comput.*, vol. 52, no. 186, 675–714, 1989

[9] Hill R., Shashkov M. "The symmetric Moment-of-Fluid interface reconstruction algorithm." *J. Comput. Phys.*, vol. 249, 180–184, 2013

[10] Kikinzon E., Shashkov M., Garimella R. "Establishing mesh topology in multi-material cells: Enabling technology for robust and accurate multi-material simulations." *Computers and Fluids*, vol. 172, 251–263, 2018

[11] Slutz S., Vesey R. "High-gain magnetized inertial fusion." *Phys. Rev. Letters*, vol. 108, 2012

[12] Anbarlooei H., Mazaheri K. "'Moment-of-fluid' interface reconstruction method in axisymmetric coordinates." *Int. J. Numer. Meth. Biomed. Engng.*, vol. 27, 1640–1651, 2011

[13] Diot S., Francois M., Dendy E. "An interface reconstruction method based on analytical formulae for 2D planal axisymmetric arbitrary convex cells." *J. Comput. Phys.*, vol. 275, 53–64, 2014

[14] Chen X., Zhang X. "A predicted-Newton's method for solving the interface positioning equation in the MoF method on general polyhedrons." *J. Comput. Phys.*, vol. 384, 70–76, 2019

[15] Milcen T., Lemoine A. "Moment-of-fluid analytic reconstruction on 3D rectangular hexahedrons." *J. Comput. Phys.*, vol. 409, 109346, 2020

[16] Herring A., Ferenbaugh C., Malone C., Shevitz D., Kikinzon E., Dilts G., Rakotoarivelo H., Velechovsky J., Lipnikov K., Ray N., Garimella R. "Portage: a modular remap and code link library for advanced architectures." *J. Open Research Software*, 2021

[17] Burton D. "Multidimensional discretization of conservation laws for unstructured polyhedral grids." Tech. Rep. UCRL-JC-118306, Lawrence Livermore National Laboratory, 1994

[18] Okabe A., Boots B., Sugihara K., Chiu S.N. *Concepts and Applications of Voronoi Diagrams.* John Wiley & Sons, New York, 2000

[19] Powell D., Abel T. "An exact general remeshing scheme applied to physically conservative voxelization." *J. Comput. Phys.*, vol. 297, 340–356, 2015